ACCOUNTS of chemical research

pubs.acs.org/accounts Article

Mechanochemistry of Metal−Organic Frameworks under Pressure and Shock

Xuan Zhou, Yurun Miao, Kenneth S. Suslick,* and Dana D. Dlott*

Cite This: *Acc. Chem. Res.* 2020, 53, 2806−2815 Read Online

ACCESS | Metrics & More | Article Recommendations

CONSPECTUS: Metal−organic framework solids (MOFs) are synthetic nanoporous materials that have drawn intense efforts in synthesis and characterization of chemical properties, most notably for their ability to adsorb liquids and gases. They are constructed as "node−spacer" nanostructured materials: metal centers (ions or clusters) connected by organic linkers (commonly containing carboxylate or imidazolate groups) to form crystalline, extended, often highly nanoporous structures. MOFs exhibit a variety of advantages over conventional porous materials: rationally designed synthesis of desired crystal structures and crystal engineering become feasible; great synthetic versatility and ease of incorporating different chemical functionalities are realized; and the use of lightweight organic linkers allows for ultrahigh surface area and porosity previously not accessible to conventional materials (i.e., zeolites and porous carbon). As a consequence, MOFs show great promise for a rapidly expanding collection of applications such as gas storage, separations, catalysis, sensing, and drug delivery.

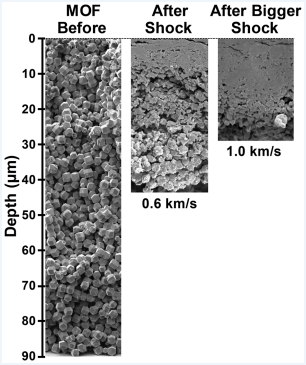

The mechanochemistry of MOFs and their response to shock waves, which we discuss in this Account, have been only partially explored. Mechanochemistry, the connection between the mechanical and the chemical worlds, has ancient origins. Rubbing sticks together to start a fire is mechanochemistry. Only in the past decade or so, however, has mechanochemistry gained a notable focus in the chemical community. In the following discussion, we present a general introduction to the complex mechanochemical behavior of MOFs both under quasi-static compression and under shock loading created by high-speed impact. During elastic deformation, MOFs undergo reversible structural or phase transitions. Plastic deformation of MOFs can result in mechanochemistry and can permanently modify the crystal structure, the pore dimensions and configuration, and the chemical bonding. The large energies required to induce bond rearrangement during plastic deformation suggest an interesting potential of MOFs for shock wave mitigation applications.

MOFs are promising materials for shock energy dissipation because of the high density of nanopores which can absorb shock energy as they collapse. We have recently developed a platform to assess shock wave energy attenuation by MOFs and other powdered materials. It uses a tabletop laser-driven flyer plate to impact MOF samples at velocities of up to 2.0 km/s. The pressure of the shock waves that break out from the MOF sample can be measured by photon Doppler velocimetry. By measuring the shock profiles of MOF layers with different thicknesses, we can determine the shock pressure attenuation by the MOF layer. We have identified the two-wave structure of shocks in MOFs caused by nanopore collapse. Electron micrographs of recovered shocked MOFs show distinct zones in the shocked material corresponding to shock powder compaction, nanopore collapse, and chemical bond destruction.

KEY REFERENCES

- Miao, Y. R.; Su, Z.; Suslick, K. S. Energy Storage during Compression of Metal−Organic Frameworks. *J. Am. Chem. Soc.* **2017**, *139*, 4667−4670.[1] *Uniaxial nanocompression of UiO-type isostructure MOFs showed that the MOFs can absorb mechanical energy of 3−4 kJ/g above 8 GPa stress. Gram for gram, this is comparable to the energy released by a TNT explosion, which is 4 kJ/g.*
- Su, Z.; Miao, Y. R.; Zhang, G. H.; Miller, J. T.; Suslick, K. S. Bond breakage under pressure in a metal organic framework. *Chem. Sci.* **2017**, *8*, 8004−8011.[2] *Observation of compression-induced endothermic chemical bond breakage in UiO-66 observed with EXAFS and IR spectroscopy.*
- Zhou, X.; Miao, Y.-R.; Shaw, W. L.; Suslick, K. S.; Dlott, D. D. Shock wave energy absorption in metal−organic framework. *J. Am. Chem. Soc.* **2019**, *141*, 2220−2223.[3] *Shock waves through ZIF-8 films are absorbed via powder compaction, nanopore collapse, and chemical bond break-*

Received: June 22, 2020
Published: September 16, 2020

https://dx.doi.org/10.1021/acs.accounts.0c00396
Acc. Chem. Res. 2020, 53, 2806−2815

age. The three mechanisms become dominant at different shock strengths.

- Banishev, A. A.; Shaw, W. L.; Bassett, W. P.; Dlott, D. D. High-speed laser-launched flyer impacts studied with ultrafast photography and velocimetry. *J. Dyn. Behav. Mater.* **2016**, *2*, 194−206.[4] *A description of the tabletop flyer plate launcher and photon Doppler velocimeter.*

1. INTRODUCTION

Metal−organic framework solids (MOFs) have metal centers (ions or clusters) connected by bifunctional organic linkers (Figure 1), forming extended crystalline structures.[5] The ease

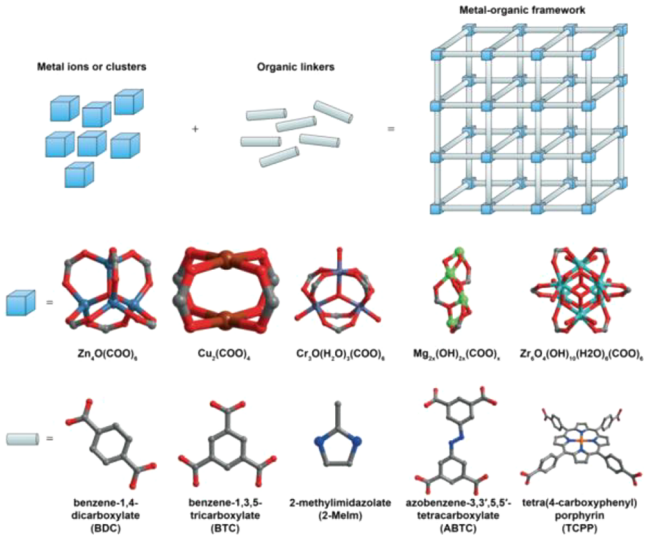

Figure 1. Node−spacer structure of MOFs and some representative metal centers and organic linkers. Reproduced with permission from ref 6. Copyright 2016 Springer Nature.

of changing the metal center or linker allows an essentially unlimited variety of rationally designed structures and engineering of materials with ultrahigh surface areas and porosities. MOFs are used in a rapidly expanding collection of applications, including gas storage and separation, catalysis, sensing, and drug delivery.

For many of these applications, mechanical stability under desolvation or repeated cycles of pressurization becomes important.[6] Mechanical properties are being studied under static high pressure, indentation, and shock compression.

Mechanochemistry[7] has ancient origins: grinding, milling, and even rubbing sticks together to start a fire are mechanochemistry. Mechanochemistry has been a notable focus in the chemical community in specialties ranging from metallurgy and polymer science to organic and inorganic synthesis and cellular biology.[7b,c,8]

Many MOF applications, such as gas adsorption, require the structure to change reversibly, while others, such as shock wave attenuation, involve plastic deformation and demolition of the MOF structure and are inherently mechanochemical events. Elastic and plastic deformations require significantly different experimental approaches.

One possible mechanochemical application of MOFs is protection of equipment or personnel from shocks produced by bombs or bullets,[9] A shock is produced by dynamic compression, for instance by impact of a projectile.[10] Shock velocities are supersonic, roughly the sum of the material velocity plus the acoustic velocity.[10] Shock measurements are simplified in the planar geometry of Figure 2a, where a shock is

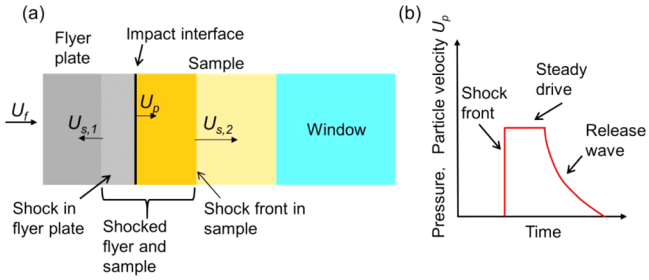

Figure 2. (a) Schematic of a planar shock produced by flyer plate impact. U_f, U_p, and U_s are the flyer plate, material flow, and shock velocities, respectively. (b) A steep shock front is followed by a steady drive and unloading when the release wave arrives.

generated by a flat impact with a "flyer plate". U_f, U_p, and U_s are the flyer plate, material flow, and is shock velocities, respectively. A planar shock has a steep shock front, a steady drive, and a release (Figure 2b). The release occurs when the back-propagating shock in the flyer reaches the free surface and the flyer stops pushing.[10]

Impacts of 0.1 to 10 km/s with solids can produce pressures of up to hundreds of gigapascals (1 GPa = 10 000 atm) and temperatures of up to thousands of kelvins. Shock wave rise times are generally nanoseconds or more but can be picoseconds in thin layers of stiff materials.[11] In solids, shocks move at speeds of kilometers per second (or equivalently, nm/ps, μm/ns, or mm/μs). A shock can travel a centimeter in a microsecond and across a molecule in a picosecond.

Other ways to attenuate a shock are to convert its forward momentum into shear waves or into heat via shock wave energy absorption. Notable shock absorption materials include sand (powder compaction) and foam (pore collapse). In MOFs, these mechanisms may be combined with endothermic bond breakage, where pore collapse may break metal−linker bonds.[12]

2. MECHANOCHEMISTRY DURING PLASTIC DEFORMATIONS

MOFs generally maintain their crystallinity with elastic deformations,[13,14] which may cause phase changes or small changes in metal ion ligation. Hydrostatic and uniaxial compression,[18a,18b] ball milling, indentation, or shock can stress MOFs beyond the elastic limit.

2.1. Amorphization and Densification of MOFs

MOF structural evolution during plastic deformation is associated with a decrease in crystallinity and porosity. Irreversible deformations are typically studied post mortem using powder X-ray diffraction[15] and gas adsorption porosimetry, but real-time methods are emerging. Friščić and coworkers studied MOFs during ball milling using synchrotron X-ray diffraction.[14c,16] Raman spectroscopy has been used to determine the reactivity of bridging carboxylate groups during pressure-induced amorphization.[17]

Ball milling of MOFs need not involve just pulverization. The mechanochemical synthesis of Zn-MOF-74 produced a dense phase before forming the porous MOF-74 framework.[16c] It was proposed that Zn first coordinated with the linker carboxylic groups and then gradually coordinated with the

https://dx.doi.org/10.1021/acs.accounts.0c00396
Acc. Chem. Res. 2020, 53, 2806−2815

phenol groups to form crystalline porous MOF-74. The metastable structure in the early stages of ball milling shows that dynamic mechanical stress may provide unique mechanochemical environments not routinely accessible by conventional chemistry.

2.2. Plastic Deformation and Mechanical Energy Absorption

When porous MOFs are immersed in fluids, compression can cause some fluids to penetrate the MOF and fill the pores, while other fluids are nonpenetrating and simply act as hydrostatic media to compress the MOF.[18] Both compression processes are nearly reversible, since the energy stored in the structure is merely tens of joules per gram. Plastic deformations that induce volume collapse can *absorb* thousands of times more energy (kJ/g),[3] which is about the same magnitude as *produced* by a gram of high explosive.[19]

2.2.1. Nanocompression of Single Crystals. The Suslick group performed nanocompression experiments using the apparatus depicted in Figure 3, which can produce uniaxial gigapascal stresses on submicron samples inside a transmission electron microscope (TEM).[20] The sample can be a single nanocrystal, which eliminates complications from interparticle interactions and macroscopic defects. Figure 4 shows simultaneous video and load−displacement data obtained by the Suslick group on a single ZIF-8 crystal.

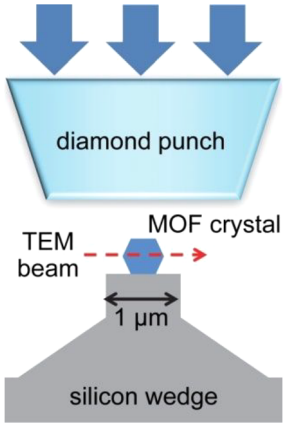

Figure 3. Nanocompression for in situ uniaxial compression within a transmission electron microscope (TEM). The loading force is measured by a piezoactuator that presses the diamond punch against the MOF crystal.

ZIF-8 is a stable MOF consisting of Zn metal centers and imidazolate linkers, and it is one of few MOFs that do not collapse when desolvated to empty the nanopores. The diamond punch (Figure 3) can continuously compress a ZIF-8 crystal without obvious cracking or fracture until the crystal is completely flattened at 4400 μN. After flattening, the punch could be retracted from the pancaked crystal (Figure 4) to reveal the extent of irreversible plastic deformation.

At each stage of compression, Young's modulus, which quantifies the relation between the stress and strain under uniaxial compression, was calculated. The loading modulus (E_{load}) of 4.6 ± 0.2 GPa is close to previous reports of 2.9−3.2 GPa for larger single crystals.[21] The unloading modulus (E_{unload}), however, is much larger (41 ± 4 GPa) because after compression the ZIF-8 has been made dense and amorphous. Experiments were also performed by filling the ZIF-8 pores with methanol, a penetrating but nominally unreactive solvent. Methanol-solvated microcrystals were brittle and shattered at quite low applied loads of 600 μN.

The Suslick group also studied four UiO-type isostructural MOFs with various linker lengths and pore sizes, as shown in Figure 5.[1] The absorbed mechanical energy can be calculated by integrating under the load−displacement curve. Figure 6 shows that the energy absorption was thousands of times larger (kJ/g) than for elastic displacements. The loading Young's modulus E_{load} decreased as the linker length increased, as expected and predicted.[22] MOF-801 was a notable exception: it was the most compressible despite having the shortest linker. This unexpected result was explained by NMR analysis of a digested MOF-801 sample, which showed a high concentration of defects (~18%) from monocarboxylate ligands (which are unfortunately required for the synthesis) that facilitated pore collapse.[1]

In all of the MOFs studied, the unloading modulus was linearly correlated with the applied maximum stress, indicating that structure densification and amorphization significantly increases the mechanical strength of these MOFs.

Figure 6 shows that in the low-stress range (<2 GPa except for MOF-801), UiO MOFs absorb small energies (a few J/g), indicating predominantly elastic deformation. The absorbed

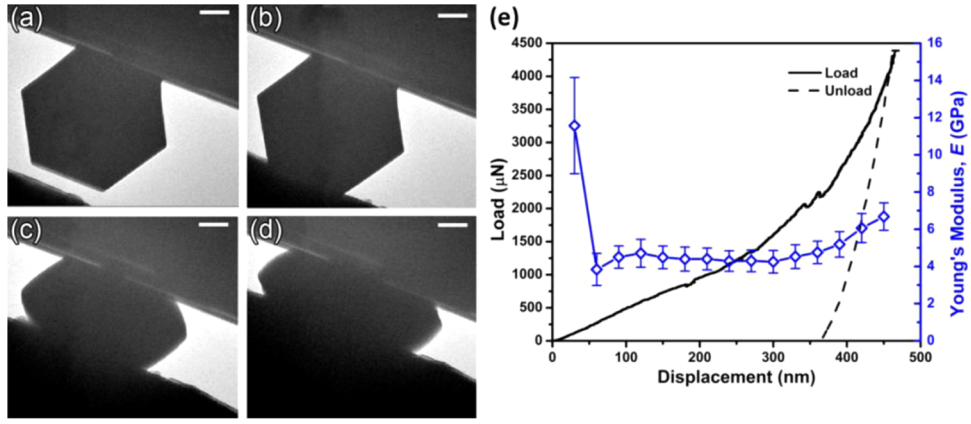

Figure 4. (a−d) In situ TEM images of a ZIF-8 microcrystal between the punch and anvil (a) without compression and at uniaxial displacements of (b) 60, (c) 270, and (d) 390 nm. Scale bars are 200 nm. (e) Load−displacement curve for a 1.2 μm ZIF-8 crystal and calculated Young's modulus vs displacement. Adapted from ref 12a. Copyright 2015 American Chemical Society.

https://dx.doi.org/10.1021/acs.accounts.0c00396
Acc. Chem. Res. 2020, 53, 2806−2815

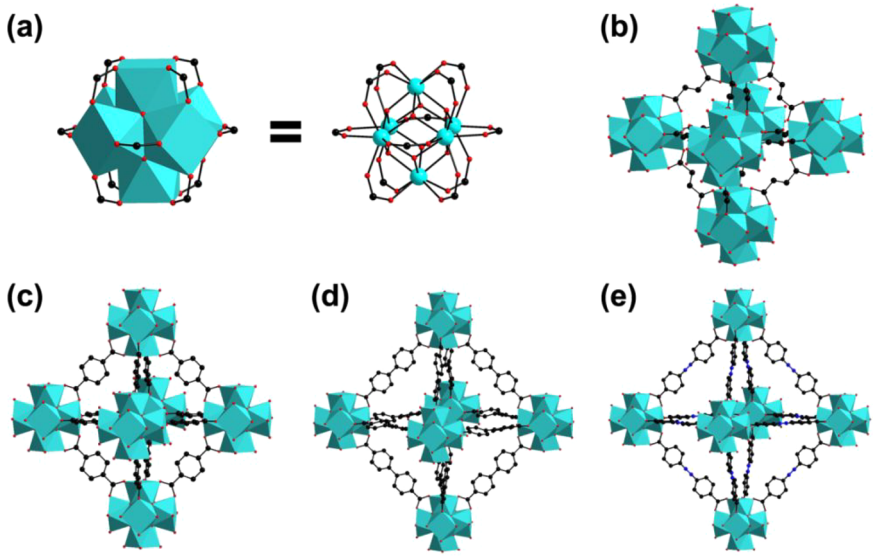

Figure 5. (a) Structure of the $Zr_6O_4(OH)_4$ cluster in UiO-type MOFs and (b–d) structures of several UiO-type MOFs: (b) MOF-801, (c) UiO-66, (d) UiO-67, and (e) UiO-abdc. Zr, turquoise; C, black; O, red; N, blue; H omitted for clarity. Adapted from ref 1. Copyright 2017 American Chemical Society.

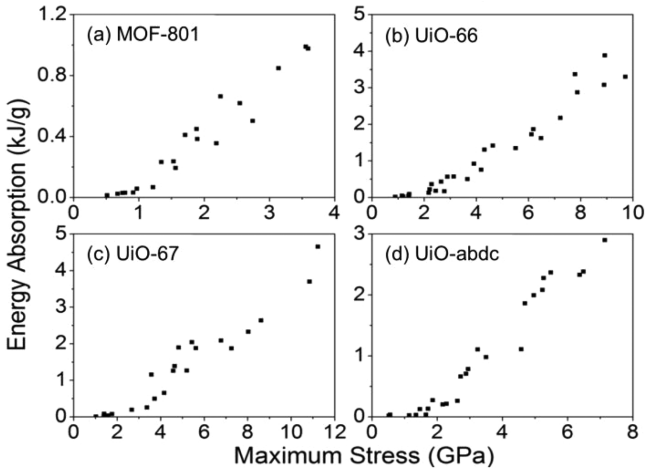

Figure 6. Mechanical energy absorption of UiO MOFs as a function of stress. Adapted from ref 1. Copyright 2017 American Chemical Society.

energy increases substantially with stresses above 2 GPa. In fact, with stresses above 8 GPa, the absorbed energy can be 3–4 kJ/g.[1] For comparison's sake, the energy released in an TNT explosion is 4 kJ/g. Gram for gram, MOFs can absorb as much energy as a high explosive can release!

The single-crystal nanocompression experiments measure normal strain and volume collapse. Since other mechanisms (e.g., powder compaction) can contribute to energy absorption, the nanocompression measurements represent a lower bound for the energy absorption capacity.

2.2.2. Mechanochemical Reactions during Nanocompression. Void collapse of compressed MOFs could be a purely physical process or a mechanochemical process. A physical mechanism might be rotation of the linker around the metal center to flatten the pores. A mechanochemical mechanism would involve breakage of the metal–linker bonds and possibly the linker itself. These possibilities can be investigated by molecular spectroscopy. The extended X-ray absorption fine structure (EXAFS) spectrum for UiO-66 (Figure 7) provides evidence for mechanochemistry. In the EXAFS, two major peaks were observed,[2] corresponding to the Zr(IV) coordination shell. Overlapping features at 1.5 and 1.8 Å correspond to $Zr-O_{\mu_3\text{-}O}$ (Zr to bridging O atom) and $Zr-O_{COO}$ (Zr to carboxylate O atom) bonds, respectively, which have different bond lengths ($Zr-O_{\mu_3\text{-}O} < Zr-O_{COO}$). The intense peak at 3.1 Å is attributed to next-nearest neighbors in the Zr···Zr shell. After compression, the EXAFS shows changes in the coordination environment around Zr(IV) in UiO-66 (Figure 7c). The peaks at 1.8 and 3.1 Å dramatically decrease, which indicates the loss of $Zr-O_{COO}$ bonds and Zr···Zr contacts. After compression at 1.9 GPa, the coordination number of $Zr-O_{COO}$ decreased from 4 to ∼2. The IR spectra confirmed loss of $Zr-O_{COO}$ through the conversion of carboxylate groups from syn–syn bridging to monodentate ligation, shown schematically in Figure 7c. The peak intensity at 1.5 Å (from the $Zr-O_{\mu_3\text{-}O}$ bonds) remained unchanged regardless of the extent of compression, implying that inner $Zr-O_{\mu_3\text{-}O}$ bonds (the core of the Zr_6O_4 cluster) were not affected by compression. Pore collapse causes Zr–O bonds between bridging terephthalates and $Zr_6O_4(OH)_4$ clusters to break. Such bond breakage is significantly endothermic and provides a chemical mechanism for enhancing shock wave absorption. Breaking these metal–linker bonds requires an estimated 2.1 kJ/g. One may conclude that $Zr-O_{COO}$ bond breakage is the primary component of the measured energies of 3–4 kJ/g absorbed during nanocompression of UiO-66.

3. SHOCK WAVES AND MOFS

The motivation for studying shock compression of MOFs is to understand how to build complex materials that combine multiple shock absorption motifs. For instance, MOFs could potentially exhibit three different modes of shock absorption:[3] (1) MOF powders could exhibit powder compaction, like sand; (2) nanoporous MOFs could exhibit pore collapse, like foam; and (3) MOFs could exhibit endothermic bond breaking to absorb shock energy. This third possibility has hardly been explored to date. All three methods convert directed kinetic

https://dx.doi.org/10.1021/acs.accounts.0c00396
Acc. Chem. Res. 2020, 53, 2806–2815

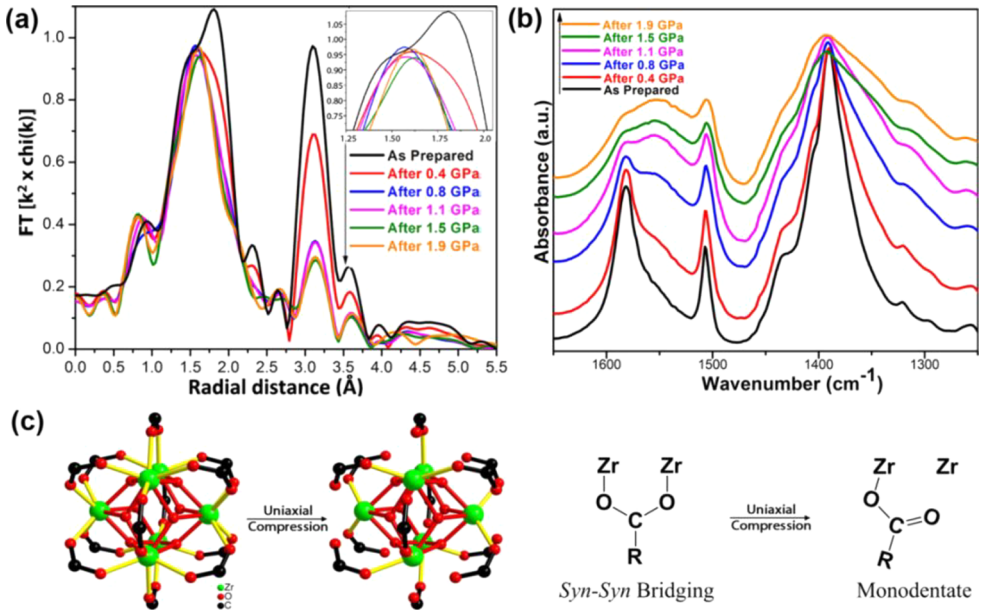

Figure 7. Bond breakage in UiO-66 after compression. (a) EXAFS spectra (magnitude of k^2-weighted Fourier transform) as prepared and after compression. Peaks that diminish upon compression at 1.8 and 3.1 Å (phase uncorrected) are attributed to Zr−O_{coo} and Zr···Zr scatterers, respectively; the unchanged peak at 1.5 Å is from Zr−$O_{\mu_3\text{-}O}$. (b) FTIR spectra of UiO-66 after compression and release; the peak shift from 1580 to 1550 cm^{-1} corresponds to the coordination mode change of carboxylate groups. (c) Change in coordination mode of bridging carboxylate within each Zr−O cluster upon compression. From ref 2. CC BY 3.0.

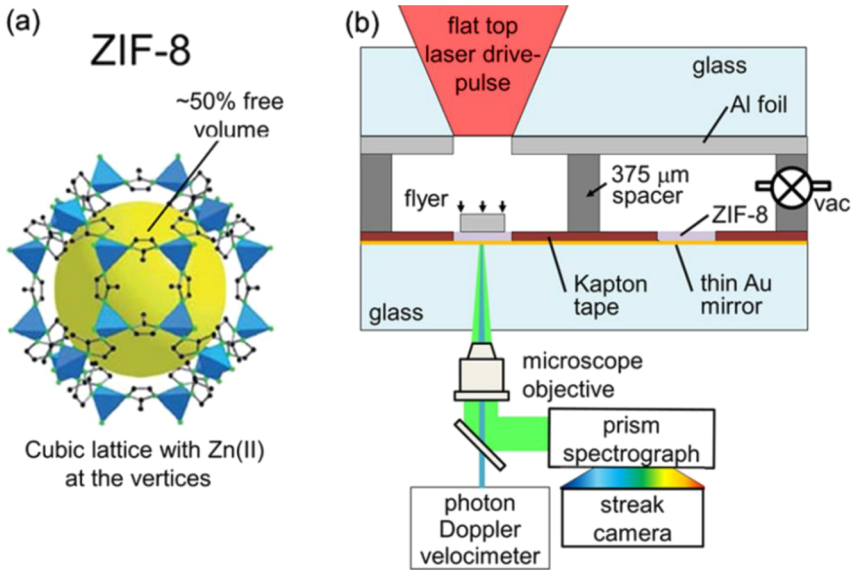

Figure 8. (a) Crystal structure of desolvated ZIF-8. The yellow ball indicates the void. (b) Schematic of the table-top laser-driven flyer plate system. Reproduced from ref 27. Copyright 2017 American Chemical Society.

energy of a shock or projectile into less harmful thermal energy. Compaction and void collapse are generally irreversible. Some of the broken bonds might spontaneously reform, transforming the shock energy into a gradual release of heat. Given the flexibility and ease of rational modification of MOF structures, these multiple mechanisms might be harnessed to develop more efficient shock absorbers.

The first shock experiments on MOFs were reported by Wei et al.[23] Large samples of a MOF called Cu-BTC were impacted by a flyer plate at pressures from 0.3 to 7.5 GPa. Post mortem X-ray diffraction revealed that the porous framework was crushed at 0.5 GPa. The inclusion of ferrocene into Cu-BTC significantly enhanced the shock resistance.

Banlusan and Strachan simulated the shock wave response of MOF-5 using molecular dynamics with a reactive force field.[24] Shocks developed a two-wave structure with an elastic wave (from the reversible part of the compression) preceding a pore-collapse wave. For impacts above 2 km/s, pore collapse was accompanied by endothermic bond breaking.

The Dlott group developed a platform to shock MOFs and study them in real time and post mortem.[3,25] As depicted in Figure 8, a tabletop laser can launch Al flyer plates[4] at MOF samples at speeds of up to 1.9 km/s. Shocked ZIF-8 (Figure

https://dx.doi.org/10.1021/acs.accounts.0c00396
Acc. Chem. Res. 2020, 53, 2806−2815

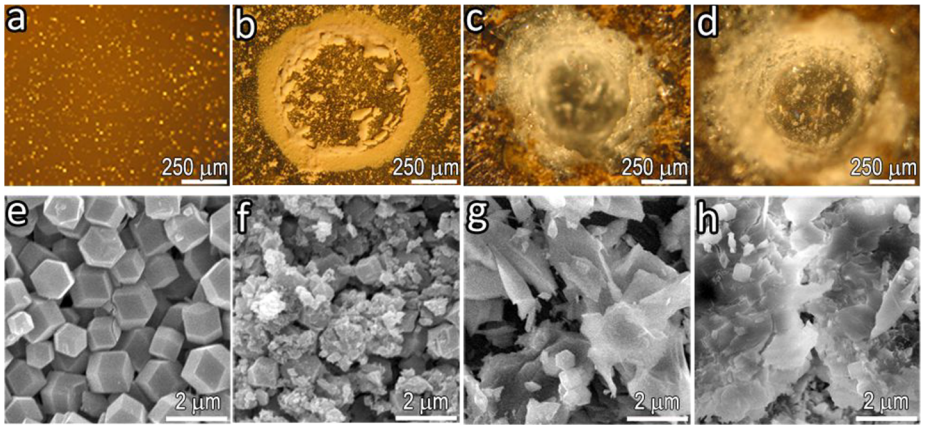

Figure 9. (top) Optical and (bottom) electron microscope images of ZIF-8 on glass: (a, e) no shock; (b, f) 0.75 km/s (2.5 GPa); (c, g) 1.3 km/s (5 GPa); (d, h) 1.6 km/s (8 GPa). Reproduced from ref 27. Copyright 2017 American Chemical Society.

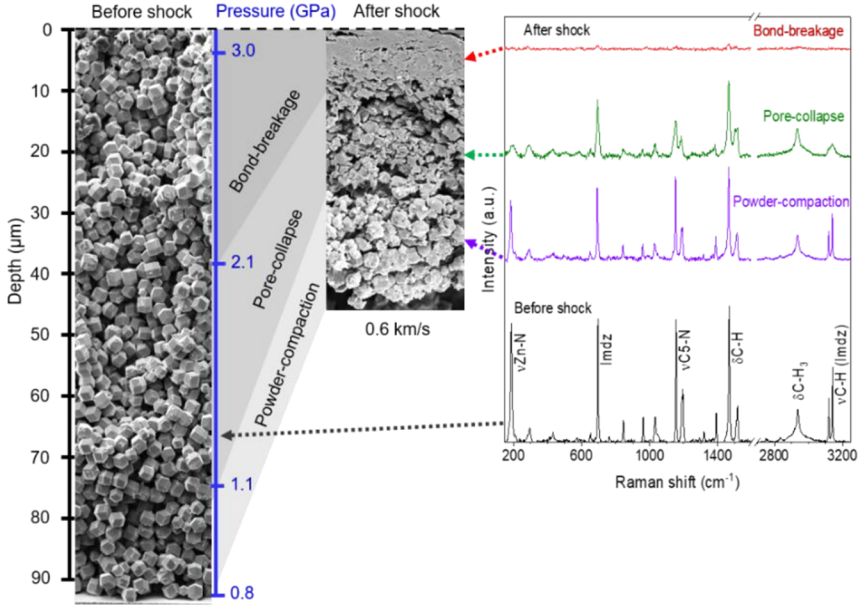

Figure 10. Cross-sectional SEM images and Raman spectra of a ZIF-8 film before and after shock compression. The shock is attenuated as it moves down the column of ZIF-8, producing three distinct zones. The Raman spectrum of each zone identifies them as amorphous material with most of the bonds broken, collapsed pores, and compacted powder. Adapted from ref 3. Copyright 2019 American Chemical Society.

8a) was studied post mortem with electron microscopy and infrared and Raman spectroscopies. A high-speed optical interferometer (photon Doppler velocimeter, PDV) measured the energies of the input and transmitted shocks to determine the shock energy absorbance.[3,26] The mechanisms of shock absorption were probed with time-resolved photoluminescence (PL) or spontaneous thermal emission.[27]

3.1. Effects of Shocks on MOFs

ZIF-8 samples were prepared as a nominally uniform layer of microcrystals with 5% polymer binder on a 50 mm × 50 mm glass window. Each of these samples could be shocked hundreds of times by moving the target area. Figure 9 shows postimpact images after impacts at several velocities. ZIF-8 crystals, initially micrometer-sized rhombic dodecahedra (Figure 9e), were damaged by compaction, fracture, fragmentation, and sintering.

Post mortem studies with X-ray diffraction and FTIR spectroscopy showed that even at lower impact velocities the crystallinity was lost but the linker groups remained intact.[27] New bands in the FTIR spectra, however, indicated that organic linker symmetry had been lowered.[27]

We were also able to obtain images and vibrational spectra from cross sections of shocked samples.[3] When the flyer plate impacted the ZIF-8 sample, it often bounced off and took ZIF-8 with it, so we could recover a stack of compressed ZIF-8 attached to a used flyer plate and study it with electron microscopy and Raman spectroscopy. We observed highly damaged ZIF-8 adjacent to the flyer plate where the shock was the strongest and less damaged ZIF-8 downstream. One example is shown in Figure 10 with a flyer plate impact at 0.6 km/s.

The preshock image in Figure 10 shows a column of loosely packed ZIF-8 crystals. After impact, the column was compressed to about half its original length. We identified three zones of damaged ZIF-8 corresponding to different shock pressures. ZIF-8 in the first zone adjacent to the flyer impact, where the pressure was the greatest, was highly compacted and essentially amorphous. As the shock was attenuated moving down the column, ZIF-8 in the second zone was pulverized.

https://dx.doi.org/10.1021/acs.accounts.0c00396
Acc. Chem. Res. 2020, 53, 2806−2815

Farther down the column in the third zone, ZIF-8 was a partially compacted mass that retained some of the original crystallite shapes. Below the third zone (not shown), ZIF-8 was undamaged.[3]

Raman microscopy was used to characterize the shocked ZIF-8 in the different zones, as shown in Figure 10. The Raman spectrum in the third zone with the weakest shock was largely unchanged from the native spectrum. Although crystals were compacted and damaged to a degree, the underlying nanoporous structure remained. In the second zone, which experienced a stronger shock, the transition near 200 cm^{-1} assigned to metal−linker bond stretching was drastically weakened, while the remainder of the spectrum corresponding to linker group vibrations was largely unaffected. In the second zone, pores were collapsed accompanied by metal−linker bond cleavage, while the linkers themselves were hardly affected. In the first zone, where the shock was hardly attenuated, no vibrational transitions were observed, indicating that the MOF was demolished, the pores were collapsed, and the linkers were destroyed.[3]

Because we could measure both material and shock velocities with PDV, we could determine shock pressure thresholds for pore collapse and molecular destruction. These thresholds, as indicated in Figure 10, were about 1.1 and 2.1 GPa, respectively.[3] A caution is that such thresholds depend on the shock duration, with longer-duration shocks being more destructive. The shock duration used here, with 75 μm thick Al flyer plates, was about 12 ns.

3.2. Real-Time Measurements on Shocked MOFs

We probed the linker groups during shock compression using their photoluminescence (PL) produced by 351 nm laser pulses that were 200 ns in duration.[27] We observed emission at 460 nm, which corresponds to the $\pi-\pi^*$ transition of the 2-MeIm linker. For impacts <1.6 km/s, this signal was unaffected by shock,[27] but above 1.6 km/s the emission instantaneously vanished, indicating that the 2-MeIm linker was damaged.

Surprisingly, in the absence of laser excitation, the shocked ZIF-8 samples spontaneously emitted an intense burst of red light long after the shock had passed, beginning about 50 ns after impact.[27] This light burst was attributed to emission produced as the high-energy chemical species created by mechanochemistry relaxed into more stable structures. These real-time optical studies showed that part of the shock energy was used to break chemical bonds, which created a stew of energetic species that gradually released thermal energy after the shock had passed.[27]

We could measure shock waves transmitted through ZIF-8 layers by coating the glass substrate (Figure 2) with a thin Au mirror.[25,28] As the shock emerged ("broke out") from the ZIF-8, it caused the ZIF-8−mirror interface to move, and that movement was recorded by the PDV high-speed interferometer. The shock energy could then be computed, since the shock equation of state, the Hugoniot equation, is known for Pyrex glass.[28] An example is shown in Figure 11 where the impact was 0.6 km/s and a series of ZIF-8 samples of different thicknesses were used to probe how the shock waveform evolved in ZIF-8. The shock profile exiting ZIF-8 has the two-wave structure characteristic of pore collapse, as simulated by Banlusan and Strachan.[29]

3.3. Shock Wave Absorption

The ability to measure shock velocity profiles and energies as the shock propagates through MOF layers with various

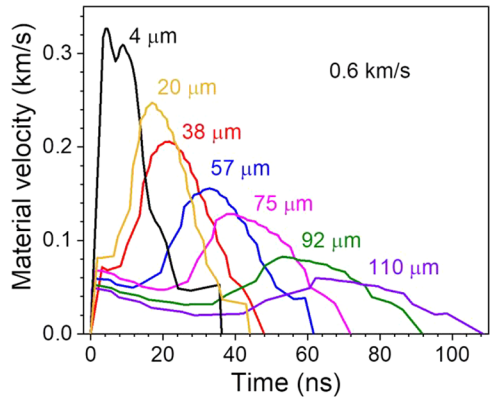

Figure 11. Shocks from a 0.6 km/s impact breaking out of different thicknesses of ZIF-8 into glass show a two-wave structure consisting of an elastic precursor and a pore collapse wave. Reprinted from ref 3. Copyright 2019 American Chemical Society.

thicknesses allows us to measure absorbance versus sample thickness (Figure 11).[3,25] In addition, our recent measurements suggest the possibility of a global method for characterizing shock wave absorption, analogous to Lambert's law for optical absorption.[25] Lambert's law states that the absorbance A of shock wave energy in a material is proportional to its thickness l,

$$A = -\log_{10}\left(\frac{F}{F_0}\right) = \frac{\alpha l}{2.303} \tag{1}$$

The Beer−Lambert law, which is more familiar to chemists, states that the absorbance is additionally proportional to the solution concentration. In eq 1, the shock energy is expressed in terms of the shock energy fluence, which is the mechanical energy passing through a unit area (e.g., kJ/m^2). F_0 is the input fluence, and F is the fluence exiting the sample after a distance l. The shock wave absorption coefficient is α. If Lambert's law applies to shock waves, then the shock wave energy transmitted through a known thickness l of material can be predicted using

$$\frac{F}{F_0} = e^{-\alpha l} \tag{2}$$

We found that we had to modify the absorption coefficient α in Lambert's law to account for energy saturation of the shocked material.[25] After a shock has compressed the pores and broken the bonds, the shocked material can hardly absorb more energy. By analogy with standard optical saturation theory,

$$A = \frac{\alpha l}{2.303} = \frac{\alpha_0 l}{2.303(1 + F/F_{sat})} \tag{3}$$

where α_0 is the unsaturated absorption coefficient and F_{sat} is the saturation fluence. The 1 in eq 3 is specific for two-level optical saturation, where $F = F_{sat}$ reduces the absorbance by a factor of 2. A different value might be needed for shock wave absorption, which is not a simple two-level system.[25]

The problem with applying eqs 1 and 2 to shock waves rather than light is determining the input and output shock wave energy fluences. For the input fluence F_0, we know the kinetic energy and area of the flyer plate striking the sample, but we do not know what fraction of that energy is transmitted to the sample. Some of the energy ends up as a shock in the

https://dx.doi.org/10.1021/acs.accounts.0c00396
Acc. Chem. Res. 2020, 53, 2806−2815

flyer plate (Figure 2a). This is analogous to correcting an absorbance spectrum for the reflection of incoming light. We approximated F_0 as the shock emerging from the thinnest sample we could practically make, which was about 4 μm thick.[25] This approximation becomes more accurate for samples thicker than 4 μm. We then measured shock fluences using PDV to measure the velocity the shock imparts to the mirrored glass substrate and deduced the shock strength in the MOF from the Hugoniot equations of state for the MOF and glass.[25,28]

The Lambert law with saturation model was tested on a variety of films consisting of ZIF-8 crystals, graphene nanoplatelets, Al, and Al_2O_3, all with 5% polymer binder. These powder films were shocked at impact velocities of 0.6–1.9 km/s (up to 14 GPa), and the results are shown in Figure 12. These shock pressures were far below the phase transition pressures of Al (217 GPa)[30] and Al_2O_3 (80 GPa)[31] but close to that of the MOF (5 GPa)[24,27] and graphene nanoplatelets (15 GPa).[32]

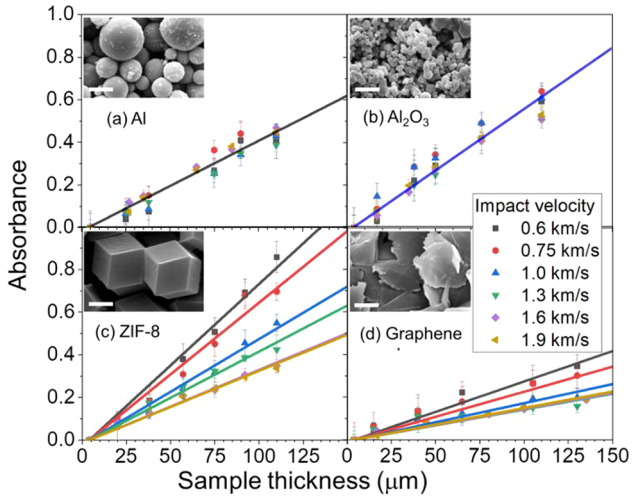

Figure 12. Shock energy absorbance versus sample thickness and electron micrographs of four powdered materials. For (a) Al and (b) Al_2O_3, the absorbance was proportional to the thickness, and Lambert's law was obeyed. For (c) ZIF-8 and (d) graphene, Lambert's law was obeyed, but the absorbance decreased with increasing shock strength, indicating absorption saturation. Scale bars represent 1 μm.

Figure 12 shows that Lambert's law was obeyed by Al and Al_2O_3 powders, where the absorbance was proportional to the sample thickness. For ZIF-8 and graphene, the data had to be fit by Lambert's law *with saturation*. Although at every flyer speed the absorbance was proportional to the sample thickness, the absorbance decreased with increasing flyer speed. After the higher-speed flyer plates have crushed and amorphized the sample, the remaining energy absorption capacity, based on the nanocompression measurements, should be on the order of joules per gram rather than kilojoules per gram. The saturation fluence for ZIF-8 needed to fit the data in Figure 12c was about 70 kJ/m^2.[25]

Lightweight materials are preferred for shock protection applications: armor must not be too heavy. For that reason, we introduced a specific absorption coefficient, which is the shock energy absorption per unit mass.[25] When we corrected for density, ZIF-8 was by far the best shock wave absorber, at least below its saturation limit, where it has a specific absorption coefficient of 55 m^2/kg.[25] To put this into perspective, we compared ZIF-8 with Plexiglas, which is used to make "bulletproof" glass. ZIF-8 turned out to absorb 7 times more shock energy than an equivalent mass of Plexiglas.[3]

4. CONCLUSIONS

Nanoporous MOFs have found myriad practical applications, including storage and separation of gases and liquids. Such applications rely on the ability of MOFs to absorb and release fluids reversibly over many cycles. Often, however, the structural changes that accompany fluid storage are not entirely reversible, and the MOF structure may break down after multiple cycles. The lack of reversibility occurs because the MOF structural changes are not entirely elastic: there is a degree of plastic deformation.

In this Account, we have focused on *irreversible* structural changes caused by plastic deformation. In particular, we have looked at how MOFs respond to gradual nanocompression and to high-speed shock compression and discovered that MOFs absorb enormous amounts of energy during compression. With gradual compression, a MOF compresses like a sponge until most of the pores have collapsed, and then the MOF becomes hard. Filling the pores with a liquid solvate makes the MOF lose its spongelike nature entirely, and it becomes brittle. Significantly, MOF compression has been shown to be a *mechanochemical* process. Post mortem EXAFS studies of the metal centers showed bond breakage and lowering of the coordination number, and FTIR spectroscopy showed changes in the local symmetry of the linker ligands.

Shock compression produces fast large-amplitude compression of the MOF structure. Besides being a particularly interesting case for study, MOFs are promising shock energy absorption media. To realize the promise of MOFs and related structures, we have developed new experimental tools to study the effects of shocks on MOFs in real time on a tabletop. We developed a laser-launched flyer plate apparatus that could deliver controlled high-speed planar impacts on MOF samples, which allowed us to examine shock effects in real time and post mortem. Our studies validated the idea that efficient shock-absorbing materials could be produced by materials having multiple mechanisms for shock absorption, including mechanochemistry. We have shown that MOFs can attenuate shock energy in three ways: powder compaction, nanopore collapse, and endothermic bond breakage, with the net result that one MOF, ZIF-8, was shown to absorb 7 times more than a common standard, Plexiglas. In fact, from experimental measurements, 1 g of ZIF-8 can absorb all of the energy released by the detonation of 1 g of TNT explosive.

Although there are likely many structural motifs that could perform as multimechanism shock absorbers, MOFs are especially useful because their modular structures lend themselves to rational synthesis and design of new structures. We have developed new tools needed to assess, understand, and predict shock absorption. We have shown that it is possible to measure shock absorption in relatively small quantities (milligrams) of precious candidate materials, and on the basis of such measurements we have developed a theoretical understanding of shock absorption analogous to Lambert's law used to analyze optical absorption.

The development of nanocompression and shock compression techniques suitable for studying plastic deformation of small quantities of interesting materials is a substantial advance toward our goal of understanding and controlling large-

https://dx.doi.org/10.1021/acs.accounts.0c00396
Acc. Chem. Res. 2020, 53, 2806–2815

amplitude deformations that are inevitably accompanied by chemical events, that is to say, mechanochemistry.

AUTHOR INFORMATION

Corresponding Authors

Dana D. Dlott − *School of Chemical Sciences, University of Illinois at Urbana−Champaign, Urbana, Illinois 61801, United States;* orcid.org/0000-0001-8719-7093; Email: dlott@illinois.edu

Kenneth S. Suslick − *School of Chemical Sciences, University of Illinois at Urbana−Champaign, Urbana, Illinois 61801, United States;* orcid.org/0000-0001-5422-0701; Email: ksuslick@illinois.edu

Authors

Xuan Zhou − *School of Chemical Sciences, University of Illinois at Urbana−Champaign, Urbana, Illinois 61801, United States;* orcid.org/0000-0002-4143-0248

Yurun Miao − *School of Chemical Sciences, University of Illinois at Urbana−Champaign, Urbana, Illinois 61801, United States*

Complete contact information is available at: https://pubs.acs.org/10.1021/acs.accounts.0c00396

Notes

The authors declare no competing financial interest.

Biographies

Xuan Zhou is a postdoctoral researcher in the Department of Chemistry at the University of Illinois at Urbana−Champaign (UIUC). She received her B.S. in Materials Physics from Xi'an Jiaotong University in China in 2009 and her Ph.D. in Optics and Nanotechnology from the Université de Technologie de Troyes in France in 2014. Her research interests include shock waves, photoelectrocatalysis, nano-optics, and photopolymerization.

Yurun Miao is currently a postdoctoral researcher with Prof. Michael Tsapatsis at the Institute for NanoBioTechnology at Johns Hopkins University. He received his B.S. from Nanjing University in China in 2012 and his Ph.D. in Chemistry from UIUC in 2017. His research interests include MOFs, amorphous materials, and mechanochemistry.

Kenneth S. Suslick is the Marvin T. Schmidt Research Professor of Chemistry at UIUC. He received his B.S. from Caltech in 1974 and his Ph.D. from Stanford in 1978 and came to Illinois immediately thereafter. He is a Fellow of the National Academy of Inventors.

Dana D. Dlott is the William H. and Janet G. Lycan Research Professor of Chemistry at UIUC. He received his A.B. from Columbia University in 1974 and his Ph.D. from Stanford University in 1979 prior to joining the faculty at Illinois. He is a past chair of the APS Topical Group on Shock Compression of Condensed Matter. He is a fellow of the American Physical Society, the American Association for the Advancement of Science, and the Optical Society of America.

ACKNOWLEDGMENTS

The research described in this study was based on work supported by the U.S. Office of Naval Research under Grant N000141210828 and by the Air Force Office of Scientific Research under Grant FA9550-19-0227. Some of the sample preparation and post mortem analysis were performed at the Frederick Seitz Materials Research Laboratory Central Facilities and the Beckman Institute at the University of Illinois at Urbana−Champaign.

REFERENCES

(1) Miao, Y. R.; Su, Z.; Suslick, K. S. Energy Storage during Compression of Metal−Organic Frameworks. *J. Am. Chem. Soc.* **2017**, *139* (13), 4667−4670.

(2) Su, Z.; Miao, Y. R.; Zhang, G. H.; Miller, J. T.; Suslick, K. S. Bond breakage under pressure in a metal organic framework. *Chem. Sci.* **2017**, *8* (12), 8004−8011.

(3) Zhou, X.; Miao, Y.-R.; Shaw, W. L.; Suslick, K. S.; Dlott, D. D. Shock wave energy absorption in metal−organic framework. *J. Am. Chem. Soc.* **2019**, *141* (6), 2220−2223.

(4) Banishev, A. A.; Shaw, W. L.; Bassett, W. P.; Dlott, D. D. High-speed laser-launched flyer impacts studied with ultrafast photography and velocimetry. *J. Dyn. Behav. Mater.* **2016**, *2* (1), 194−206.

(5) (a) Furukawa, H.; Cordova, K. E.; O'Keeffe, M.; Yaghi, O. M. The chemistry and applications of metal-organic frameworks. *Science* **2013**, *341* (6149), 1230444. (b) Zhou, H.-C.; Kitagawa, S. Metal−organic frameworks (MOFs). *Chem. Soc. Rev.* **2014**, *43* (16), 5415−5418. (c) Zhou, H. C.; Long, J. R.; Yaghi, O. M. Introduction to Metal−Organic Frameworks. *Chem. Rev.* **2012**, *112* (2), 673−674. (d) Furukawa, S.; Reboul, J.; Diring, S.; Sumida, K.; Kitagawa, S. Structuring of metal-organic frameworks at the mesoscopic/macroscopic scale. *Chem. Soc. Rev.* **2014**, *43* (16), 5700−5734. (e) Cui, Y. J.; Li, B.; He, H. J.; Zhou, W.; Chen, B. L.; Qian, G. D. Metal−Organic Frameworks as Platforms for Functional Materials. *Acc. Chem. Res.* **2016**, *49* (3), 483−493. (f) Herm, Z. R.; Bloch, E. D.; Long, J. R. Hydrocarbon Separations in Metal−Organic Frameworks. *Chem. Mater.* **2014**, *26* (1), 323−338. (g) Kreno, L. E.; Leong, K.; Farha, O. K.; Allendorf, M.; Van Duyne, R. P.; Hupp, J. T. Metal−Organic Framework Materials as Chemical Sensors. *Chem. Rev.* **2012**, *112* (2), 1105−1125. (h) Suslick, K. S.; Bhyrappa, P.; Chou, J. H.; Kosal, M. E.; Nakagaki, S.; Smithenry, D. W.; Wilson, S. R. Microporous porphyrin solids. *Acc. Chem. Res.* **2005**, *38* (4), 283−291. (i) Kosal, M. E.; Chou, J. H.; Wilson, S. R.; Suslick, K. S. A functional zeolite analogue assembled from metalloporphyrins. *Nat. Mater.* **2002**, *1* (2), 118−121.

(6) Howarth, A. J.; Liu, Y.; Li, P.; Li, Z.; Wang, T. C.; Hupp, J. T.; Farha, O. K. Chemical, thermal and mechanical stabilities of metal−organic frameworks. *Nat. Rev. Mater.* **2016**, *1*, 15018.

(7) (a) Takacs, L. The historical development of mechanochemistry. *Chem. Soc. Rev.* **2013**, *42* (18), 7649−7659. (b) Beyer, M. K.; Clausen-Schaumann, H. Mechanochemistry: The mechanical activation of covalent bonds. *Chem. Rev.* **2005**, *105* (8), 2921−2948. (c) Boldyreva, E. Mechanochemistry of inorganic and organic systems: what is similar, what is different? *Chem. Soc. Rev.* **2013**, *42* (18), 7719−7738.

(8) (a) Friscic, T.; James, S. L.; Boldyreva, E. V.; Bolm, C.; Jones, W.; Mack, J.; Steed, J. W.; Suslick, K. S. Highlights from Faraday discussion 170: Challenges and opportunities of modern mechanochemistry, Montreal, Canada, 2014. *Chem. Commun.* **2015**, *51* (29), 6248−6256. (b) Suslick, K. S. Mechanochemistry and sonochemistry: concluding remarks. *Faraday Discuss.* **2014**, *170*, 411−422. (c) May, P. A.; Moore, J. S. Polymer mechanochemistry: techniques to generate molecular force via elongational flows. *Chem. Soc. Rev.* **2013**, *42* (18), 7497−7506.

(9) Qiao, P.; Yang, M.; Bobaru, F. Impact Mechanics and High-Energy Absorbing Materials: Review. *J. Aerosp. Eng.* **2008**, *21* (4), 235−248.

(10) Forbes, J. W. *Shock Wave Compression of Condensed Matter: A Primer*; Springer Science & Business Media, 2013.

(11) Patterson, J. E.; Lagutchev, A. S.; Huang, W.; Dlott, D. D. Ultrafast dynamics of shock compression of molecular monolayers. *Phys. Rev. Lett.* **2005**, *94*, 015501.

(12) (a) Su, Z.; Miao, Y.-R.; Mao, S.-M.; Zhang, G.-H.; Dillon, S.; Miller, J. T.; Suslick, K. S. Compression-Induced Deformation of Individual Metal−Organic Framework Microcrystals. *J. Am. Chem. Soc.* **2015**, *137* (5), 1750−1753. (b) Banlusan, K.; Antillon, E.; Strachan, A. Mechanisms of Plastic Deformation of Metal−Organic Framework-5. *J. Phys. Chem. C* **2015**, *119* (46), 25845−25852.

(13) Wachtman, J. B.; Cannon, W. R.; Matthewson, M. J. Stress and Strain. In *Mechanical Properties of Ceramics*; John Wiley & Sons, 2009; pp 1−25.
(14) (a) Spencer, E. C.; Kiran, M. S.; Li, W.; Ramamurty, U.; Ross, N. L.; Cheetham, A. K. Pressure-Induced Bond Rearrangement and Reversible Phase Transformation in a Metal−Organic Framework. *Angew. Chem., Int. Ed.* **2014**, *53* (22), 5583−5586. (b) Spencer, E. C.; Angel, R. J.; Ross, N. L.; Hanson, B. E.; Howard, J. A. K. Pressure-Induced Cooperative Bond Rearrangement in a Zinc Imidazolate Framework: A High-Pressure Single-Crystal X-Ray Diffraction Study. *J. Am. Chem. Soc.* **2009**, *131* (11), 4022−4026. (c) Užarević, K.; Halasz, I.; Friščić, T. Real-Time and In Situ Monitoring of Mechanochemical Reactions: A New Playground for All Chemists. *J. Phys. Chem. Lett.* **2015**, *6* (20), 4129−4140.
(15) (a) Bennett, T. D.; Cheetham, A. K. Amorphous Metal−Organic Frameworks. *Acc. Chem. Res.* **2014**, *47* (5), 1555−1562. (b) Bennett, T. D.; Tan, J.-C.; Yue, Y.; Baxter, E.; Ducati, C.; Terrill, N. J.; Yeung, H. H. M.; Zhou, Z.; Chen, W.; Henke, S.; Cheetham, A. K.; Greaves, G. N. Hybrid glasses from strong and fragile metal-organic framework liquids. *Nat. Commun.* **2015**, *6*, 8079.
(16) (a) Halasz, I.; Kimber, S. A. J.; Beldon, P. J.; Belenguer, A. M.; Adams, F.; Honkimäki, V.; Nightingale, R. C.; Dinnebier, R. E.; Friščić, T. In situ and real-time monitoring of mechanochemical milling reactions using synchrotron X-ray diffraction. *Nat. Protoc.* **2013**, *8* (9), 1718−1729. (b) Katsenis, A. D.; Puškarić, A.; Štrukil, V.; Mottillo, C.; Julien, P. A.; Užarević, K.; Pham, M.-H.; Do, T.-O.; Kimber, S. A. J.; Lazić, P.; Magdysyuk, O.; Dinnebier, R. E.; Halasz, I.; Friščić, T. In situ X-ray diffraction monitoring of a mechanochemical reaction reveals a unique topology metal-organic framework. *Nat. Commun.* **2015**, *6*, 6662. (c) Julien, P. A.; Užarević, K.; Katsenis, A. D.; Kimber, S. A. J.; Wang, T.; Farha, O. K.; Zhang, Y.; Casaban, J.; Germann, L. S.; Etter, M.; Dinnebier, R. E.; James, S. L.; Halasz, I.; Friščić, T. In Situ Monitoring and Mechanism of the Mechanochemical Formation of a Microporous MOF-74 Framework. *J. Am. Chem. Soc.* **2016**, *138* (9), 2929−2932.
(17) Hu, Y. H.; Zhang, L. Amorphization of metal-organic framework MOF-5 at unusually low applied pressure. *Phys. Rev. B: Condens. Matter Mater. Phys.* **2010**, *81* (17), 174103.
(18) (a) Chapman, K. W.; Halder, G. J.; Chupas, P. J. Guest-Dependent High Pressure Phenomena in a Nanoporous Metal−Organic Framework Material. *J. Am. Chem. Soc.* **2008**, *130* (32), 10524−10526. (b) Graham, A. J.; Allan, D. R.; Muszkiewicz, A.; Morrison, C. A.; Moggach, S. A. The Effect of High Pressure on MOF-5: Guest-Induced Modification of Pore Size and Content at High Pressure. *Angew. Chem., Int. Ed.* **2011**, *50* (47), 11138−11141. (c) Hobday, C. L.; Marshall, R. J.; Murphie, C. F.; Sotelo, J.; Richards, T.; Allan, D. R.; Duren, T.; Coudert, F. X.; Forgan, R. S.; Morrison, C. A.; Moggach, S. A.; Bennett, T. D. A Computational and Experimental Approach Linking Disorder, High-Pressure Behavior, and Mechanical Properties in UiO Frameworks. *Angew. Chem., Int. Ed.* **2016**, *55* (7), 2401−5. (d) Graham, A. J.; Banu, A.-M.; Düren, T.; Greenaway, A.; McKellar, S. C.; Mowat, J. P. S.; Ward, K.; Wright, P. A.; Moggach, S. A. Stabilization of Scandium Terephthalate MOFs against Reversible Amorphization and Structural Phase Transition by Guest Uptake at Extreme Pressure. *J. Am. Chem. Soc.* **2014**, *136* (24), 8606−8613. (e) Moggach, S. A.; Bennett, T. D.; Cheetham, A. K. The Effect of Pressure on ZIF-8: Increasing Pore Size with Pressure and the Formation of a High-Pressure Phase at 1.47 GPa. *Angew. Chem., Int. Ed.* **2009**, *48* (38), 7087−7089. (f) Im, J.; Yim, N.; Kim, J.; Vogt, T.; Lee, Y. High-Pressure Chemistry of a Zeolitic Imidazolate Framework Compound in the Presence of Different Fluids. *J. Am. Chem. Soc.* **2016**, *138* (36), 11477−11480. (g) Ortiz, G.; Nouali, H.; Marichal, C.; Chaplais, G.; Patarin, J. Energetic performances of the metal-organic framework ZIF-8 obtained using high pressure water intrusion-extrusion experiments. *Phys. Chem. Chem. Phys.* **2013**, *15* (14), 4888−4891. (h) Ortiz, G.; Nouali, H.; Marichal, C.; Chaplais, G.; Patarin, J. Energetic Performances of "ZIF-71−Aqueous Solution" Systems: A Perfect Shock-Absorber with Water. *J. Phys. Chem. C* **2014**, *118* (37), 21316−21322. (i) Rodriguez, J.; Beurroies, I.; Loiseau, T.; Denoyel, R.; Llewellyn, P. L. The Direct Heat Measurement of Mechanical Energy Storage Metal−Organic Frameworks. *Angew. Chem., Int. Ed.* **2015**, *54* (15), 4626−4630. (j) Yot, P. G.; Vanduyfhuys, L.; Alvarez, E.; Rodriguez, J.; Itie, J.-P.; Fabry, P.; Guillou, N.; Devic, T.; Beurroies, I.; Llewellyn, P. L.; Van Speybroeck, V.; Serre, C.; Maurin, G. Mechanical energy storage performance of an aluminum fumarate metal-organic framework. *Chem. Sci.* **2016**, *7* (1), 446−450.
(19) Su, Z.; Shaw, W. L.; Miao, Y.-R.; You, S.; Dlott, D. D.; Suslick, K. S. Shock wave chemistry in a metal−organic framework. *J. Am. Chem. Soc.* **2017**, *139* (13), 4619−4622.
(20) Kiener, D.; Hosemann, P.; Maloy, S. A.; Minor, A. M. In situ nanocompression testing of irradiated copper. *Nat. Mater.* **2011**, *10* (8), 608−613.
(21) Tan, J. C.; Bennett, T. D.; Cheetham, A. K. Chemical structure, network topology, and porosity effects on the mechanical properties of Zeolitic Imidazolate Frameworks. *Proc. Natl. Acad. Sci. U. S. A.* **2010**, *107* (22), 9938−43.
(22) Yang, L.-M.; Ganz, E.; Svelle, S.; Tilset, M. Computational exploration of newly synthesized zirconium metal−organic frameworks UiO-66,-67,-68 and analogues. *J. Mater. Chem. C* **2014**, *2* (34), 7111−7125.
(23) Wei, Q.; Xu, H. W.; Yu, X. H.; Shimada, T.; Rearick, M. S.; Hickmott, D. D.; Zhao, Y. S.; Luo, S. N. Shock resistance of metal-organic framework Cu-1,3,5-benzenetricarboxylate with and without ferrocene inclusion. *J. Appl. Phys.* **2011**, *110* (5), 056102.
(24) Banlusan, K.; Strachan, A. Shockwave Energy Dissipation in Metal−Organic Framework MOF-5. *J. Phys. Chem. C* **2016**, *120* (23), 12463−12471.
(25) Zhou, X.; Suslick, K. S.; Dlott, D. D. Lambert's Law for Shock Wave Energy Absorption. *Appl. Phys. Lett.* **2020**, submitted.
(26) Zhou, X.; Miao, Y.-R.; Banlusan, K.; Shaw, W. L.; Strachan, A. H.; Suslick, K. S.; Dlott, D. D. Shock wave dissipation by metal organic framework. *AIP Conf. Proc.* **2017**, *1979*, 150043.
(27) Su, Z.; Shaw, W. L.; Miao, Y. R.; You, S.; Dlott, D. D.; Suslick, K. S. Shock Wave Chemistry in a Metal−Organic Framework. *J. Am. Chem. Soc.* **2017**, *139* (13), 4619−4622.
(28) Bhowmick, M.; Basset, W. P.; Matveev, S. M.; Salvati, L., III; Dlott, D. D. Optical windows as materials for high-speed shock wave detectors. *AIP Adv.* **2018**, *8* (12), 125123.
(29) Banlusan, K.; Strachan, A. Shockwave Energy Dissipation in Metal−Organic Framework MOF-5. *J. Phys. Chem. C* **2016**, *120*, 12463−12471.
(30) Akahama, Y.; Nishimura, M.; Kinoshita, K.; Kawamura, H.; Ohishi, Y. Evidence of a fcc-hcp Transition in Aluminum at Multimegabar Pressure. *Phys. Rev. Lett.* **2006**, *96* (4), 045505.
(31) Mashimo, T.; Tsumoto, K.; Nakamura, K.; Noguchi, Y.; Fukuoka, K.; Syono, Y. High-pressure phase transformation of corundum (α-Al_2O_3) observed under shock compression. *Geophys. Res. Lett.* **2000**, *27* (14), 2021−2024.
(32) Lu, S.; Yao, M.; Yang, X.; Li, Q.; Xiao, J.; Yao, Z.; Jiang, L.; Liu, R.; Liu, B.; Chen, S.; Zou, B.; Cui, T.; Liu, B. High pressure transformation of graphene nanoplates: A Raman study. *Chem. Phys. Lett.* **2013**, *585*, 101−106.

https://dx.doi.org/10.1021/acs.accounts.0c00396
Acc. Chem. Res. 2020, 53, 2806−2815